ELSEVIER

Hydroacoustic records and a numerical model of the source mechanism from the first historical eruption of Anatahan Volcano, Mariana Islands

R.P. Dziak[a,*], M. Park[b], H. Matsumoto[a], S.-K. Byun[b]

[a]Oregon State University/NOAA, Hatfield Marine Science Center, Newport, OR 97365, USA
[b]Korea Ocean Research and Development Institute, Ansan P.O. Box 29, South Korea

Abstract

Anatahan Volcano in the Commonwealth of the Northern Mariana Islands (CNMI) erupted for the first time in recorded history on 10 May 2003. The underwater acoustic records (*T*-waves) of earthquakes, explosions, and tremor produced during the eruption were recorded on a sound channel hydrophone deployed in February 2003. Acoustic propagation models show that the seismic to acoustic conversion at Anatahan is particularly efficient, aided by the upward slope of the seamount toward the hydrophone. The hydrophone records confirm the onset of earthquake activity between 0100 and 0200Z on 10 May, with a substantial increase in seismicity beginning at ~0620Z. In addition, the onset of continuous, low-frequency (3–40 Hz) acoustic energy that is likely volcanic tremor related to magma intrusion was also observed at 0620Z. The hydrophone recorded 1401 earthquakes during the first 3 days of the eruption. A histogram of seismicity indicates two main periods of explosion/eruption activity, the first beginning at ~0620Z on 10 May and the second at ~0000Z on 11 May. Relative earthquake depth estimates indicate that both eruption periods were accompanied by earthquake activity from deep within the Anatahan volcanic edifice. A numerical representation of the Anatahan volcano-seismic source was developed to examine the character of acoustic signals generated from the eruption governed by the geometry of the source and the physical properties of the magma. A magma pipe source mechanism is used to compute the seismo-acoustic wavefield on the flank of the Anatahan volcanic edifice (on the seafloor and in the water column) due to mode conversion by roughness scattering. A fluid-filled pipe model was chosen because it allows for a more straightforward relation between volcano geometry and spectral features of harmonic tremor as well as its morphologic similarity to a submerged volcanic edifice.
© 2005 Elsevier B.V. All rights reserved.

Keywords: hydrophone; earthquakes; tremor; seismo-acoustic propagation

1. Introduction

In February 2003, an array of 5 hydrophones was deployed along the active island- and back-arc of the

---

* Corresponding author.
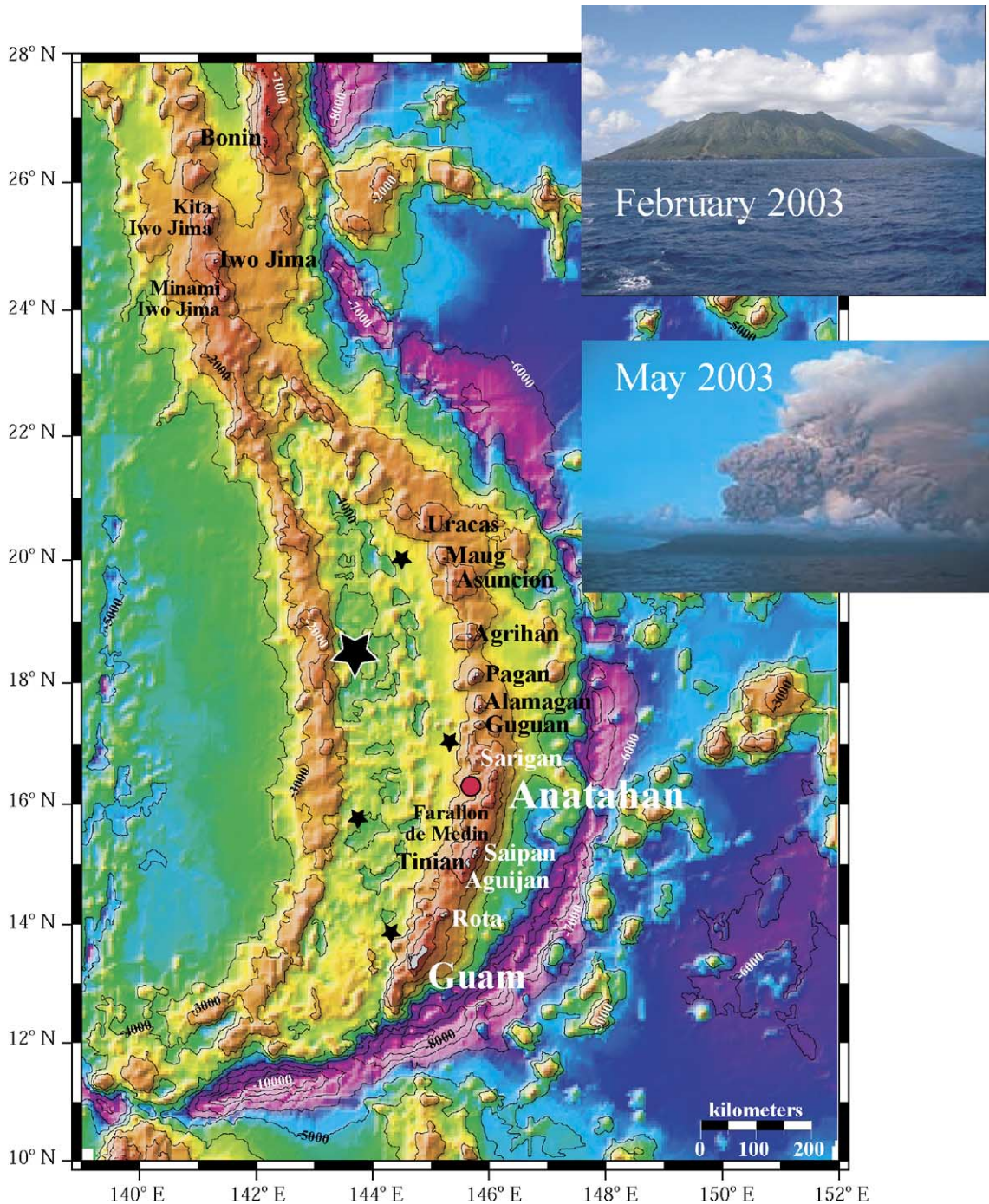   *E-mail address:* robert.p.dziak@noaa.gov (R.P. Dziak).

Fig. 1. Bathymetry of the Commonwealth of the Northern Mariana Islands with the locations of the major islands labeled. Red circle shows the location of Anatahan Island. Black stars show location of five hydrophones deployed in February and recovered in September 2003, large star indicates hydrophone that recorded data. Inset pictures show Anatahan Volcano 3 months before, and the first day of, the eruption.

Mariana Islands (Fig. 1) and moored within the ocean sound channel. The hydrophones (1–110 Hz bandpass) were designed to record the hydroacoustic tertiary phase or *T*-wave of oceanic earthquakes and estimate the acoustic location of these earthquakes from throughout the Commonwealth of the Northern Mariana Islands (CNMI). Because acoustic *T*-waves obey cylindrical spreading (r^{-1}) energy loss as opposed to the spherical spreading (r^{-2}) of solid-earth seismic *P*-waves, sound channel hydrophones can often detect smaller and therefore more numerous earthquakes than land-based seismic networks (Fox et

al., 1994). Seismic coverage in the Pacific ocean basin is sparse because permanent installations are restricted largely to islands, thereby limiting our understanding of seismicity and volcanic activity in the deep-ocean and significant portions of the Earth (Kanamori et al., 1988).

On 10 May 2003 the first documented eruption of Anatahan Volcano (in the center of the CNMI) occurred in historical time (Wiens et al., 2004). Anatahan is a composite volcano that erupts primarily dacitic lavas, and has the largest caldera of all the volcanoes in the CNMI indicating that explosive
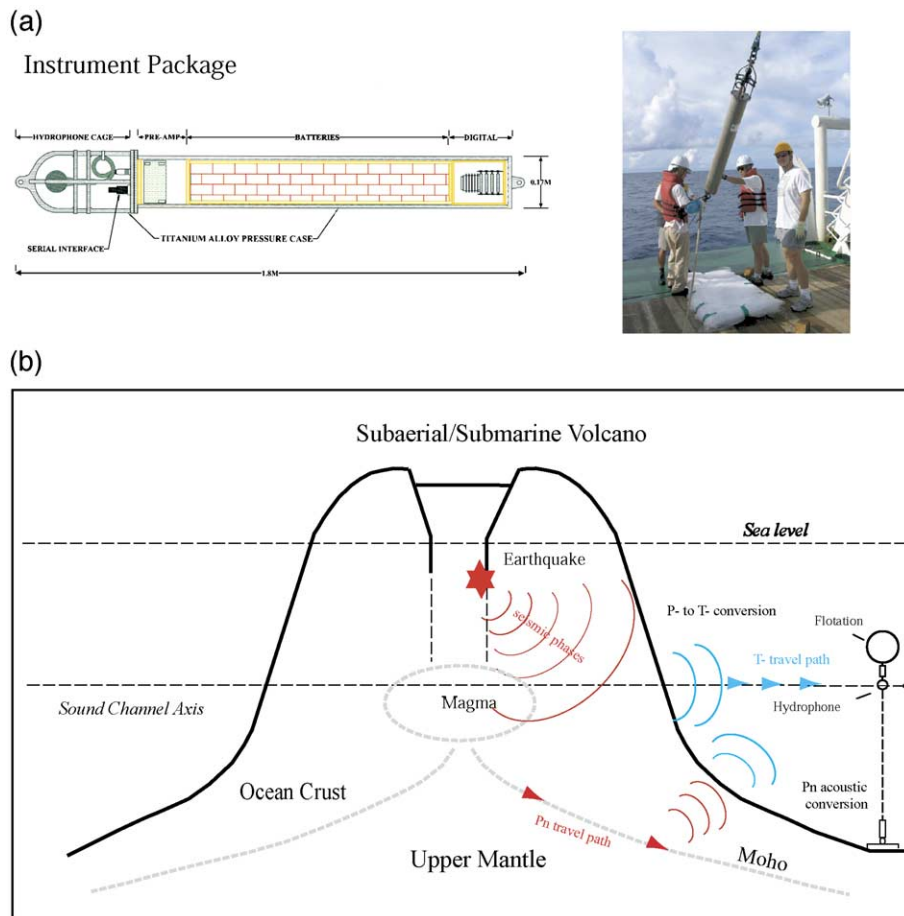

Fig. 2. Diagram showing (a) hydrophone schematics and (b) mooring design and probable seismic/acoustic propagation paths detected on the hydrophones. Pre-amplifier, digital logging section and hard drives are contained within a titanium pressure case powered by 150 D-cell batteries. The hydrophone instrument package is anchored to the seafloor then suspended in the SOFAR channel using a single large syntactic float. Earthquakes within Anatahan volcanic edifice produce seismic waves that propagate laterally through the crust and convert to an acoustic phase at the seafloor–ocean interface. This acoustic phase will then propagate into the sound channel wave-guide becoming a *T*-wave (Park and Odom, 1999). Seismic phases from this earthquake also propagate along the Moho discontinuity (*Pn*) and convert to an acoustic phase near the hydrophone.

eruptions were always a possibility (BGVN, 2003). Unfortunately, of the five hydrophones deployed during the experiment, only the hydrophone located at 18°–16.8′N, 143°–45.7′E recorded throughout the eruption of Anatahan. The data from this one hydrophone, however, provides critical information on the onset of earthquake and volcanic tremor activity related to the first few days of the eruption and on the efficiency of seismic to acoustic wave conversion for earthquakes occurring within this subaerial/submarine volcano. In addition, a numerical model of the eruption activity recorded on the hydrophone provides insight into the possible volcano source geometry and physical properties of the magma as well as the efficiency of T-wave generation from seismic wave scattering.

2. Instrument description

A schematic diagram of the autonomous hydrophone instrument and mooring is shown in Fig. 2. The hydrophone instrument package includes a single omni-directional ceramic hydrophone, a filter/amplifier stage, an accurate clock and a datalogger modified from an off-the-shelf microprocessor (Fig. 2a). The instrument is capable of recording at 16-bit data resolution at 250 Hz (1–110 Hz bandpass) for periods of up to 2.5 years. The analog filter/amplifier section is designed to pre-whiten the ocean ambient noise spectrum. The hydrophone and pre-amplifier together have a flat frequency response over the pass band, but the low-end frequency begins to roll off at 0.6 Hz. Accurate timing is provided by a software-controlled, temperature-correcting crystal oscillator with an average drift of 400 ms during a typical year-long deployment. Current disk technology allows for five 8-Gbyte capacity drives, or a total of 40-Gbyte total storage. The electronics are powered by 168 standard alkaline D-cell batteries which are replaced on the research vessel during re-deployments.

The field package includes a custom pressure case manufactured from aircraft titanium tubing which has a maximum depth rating of 1200 m. The instrument case is attached to a standard oceanographic mooring (Fig. 2b) with anchor, acoustic release, and mooring line pre-measured to place the sensor at the proper water depth within the ocean sound channel (~900–

1000 m in the Marianas region). A syntactic foam float suspends the mooring above the seafloor and keeps it under tension. A small pressure and temperature recorder is attached to the mooring line below the float to record the depth should dramatic hydrophone depth changes occur in response to stronger than normal currents.

3. Seismo-acoustic propagation

A schematic diagram of the probable seismic and acoustic propagation paths is also shown in Fig. 2b. Although Anatahan is a subaerial volcano, the vast majority of the volcanic edifice is submarine. The floor of the caldera was estimated at 68 m above sea level before the eruption, but had subsided to nearly sea level by 20 May (BGVN, 2003). Therefore many of the earthquakes related to the eruption and the ascent of magma beneath the caldera are below sea level, and much of their seismic energy will be able to project downward, and laterally, out of the volcanic edifice and into the water column. The depth of the ocean-sound channel in this region is ~800 m (Fig. 3a and b; Davis et al., 1986), and earthquakes that produce seismic waves with take-off angles that are horizontal or near to horizontal (Fig. 2b) will have the most enhanced seismic to acoustic conversion process as the waves will refract directly into the sound channel as they exit the volcanic edifice and propagate into the water column. Thus multiple seafloor–sea surface reflections are not needed to obtain a horizontal raypath to enter the sound channel (Talandier and Okal, 1998), and therefore much more of the signal's energy is preserved.

A model of the acoustic propagation loss, referred to as the Parabolic Equation model or PE (e.g. Collins, 1993), from the seafloor–ocean interface on the flank of the volcano to the hydrophone is shown in Fig. 3c. Acoustic propagation models are not designed to estimate seismic propagation in the shallow ocean crust, but this will be reconsidered in numerical models of the volcano-seismic source presented later in the text. The PE loss model was estimated assuming a source energy of 220 dB at a depth of 500 m (equivalent to a magnitude 4–5 earthquake, Fox et al., 2001), a hydrophone depth of 900 m, a
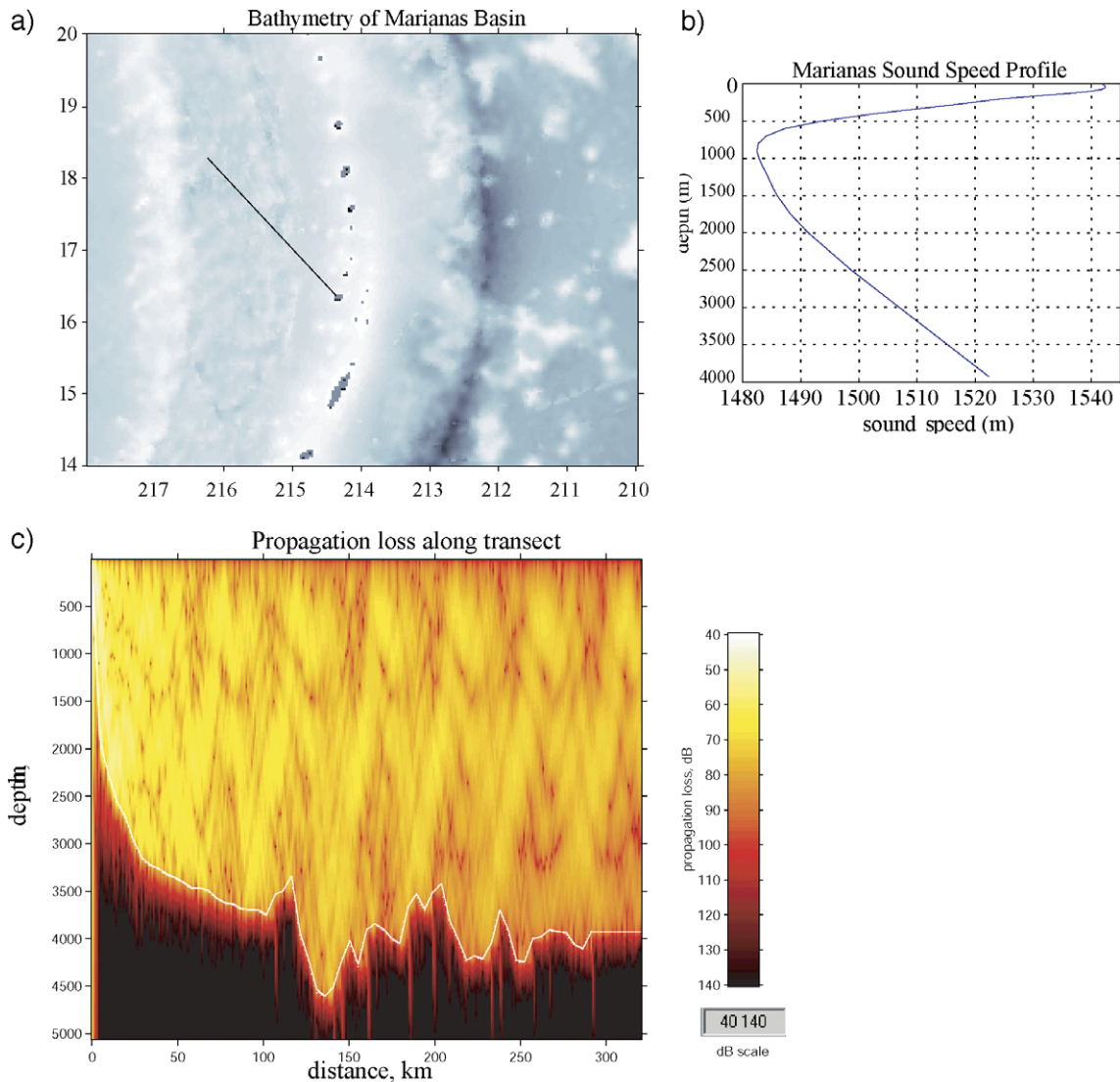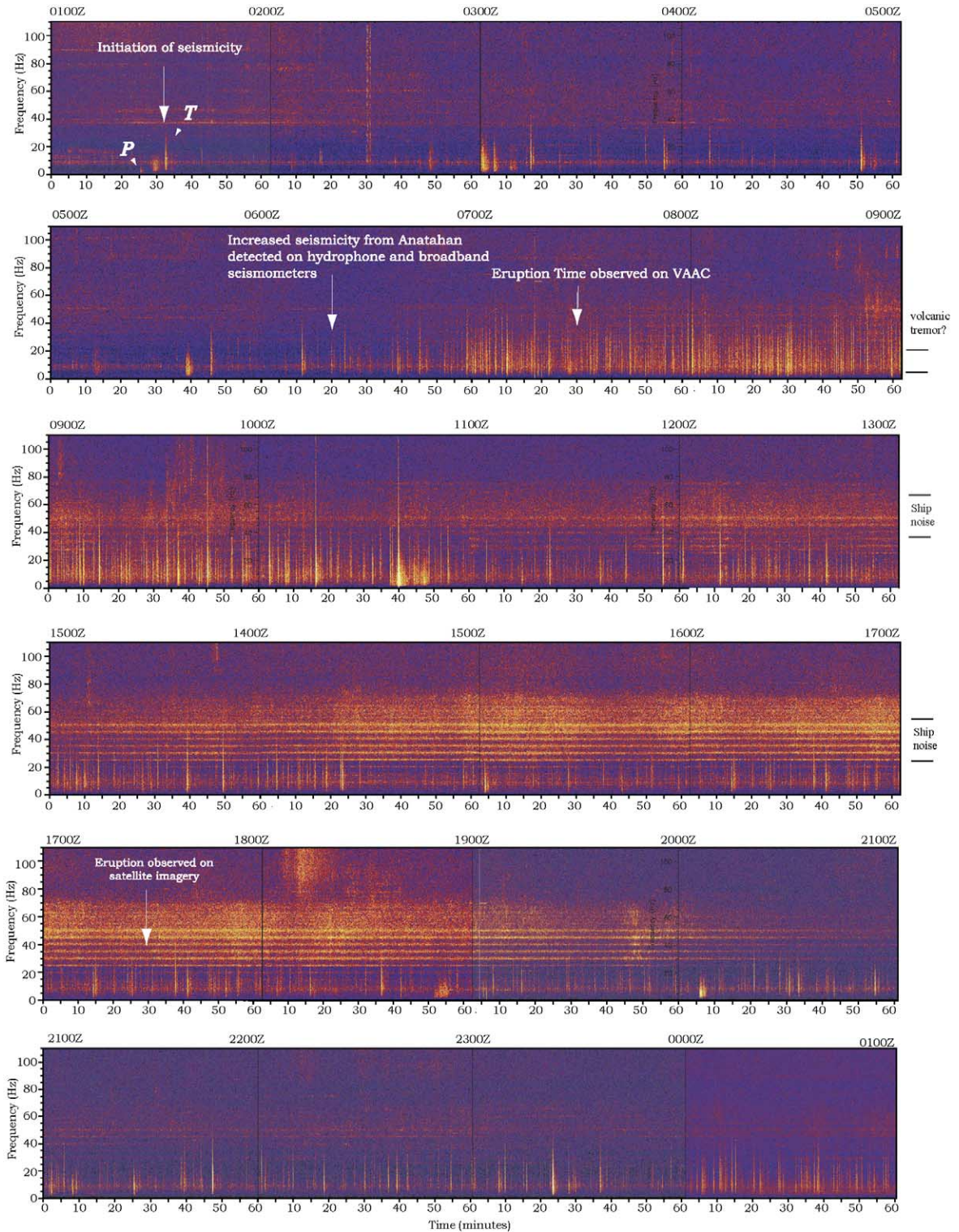
Fig. 3. The acoustic propagation path from Anatahan Volcano to the northwest hydrophone is shown in diagrams (a) and (c). The ocean sound-speed profile for the summer season at the hydrophone location is shown in diagram (b), sound channel axis is ~800 m. The water column along the path is free of obstructions (seamounts, etc.) allowing for little attenuation of signal strength. The Parabolic Equation propagation loss model (diagram c) was estimated assuming a source of 220 dB (equivalent to a M~4–5 earthquake) at a depth of 500 m on the flank of Anatahan Volcano, a receiver depth of 900 m, and the velocity model shown. The propagation loss model indicates the expected attenuation along the path is relatively low (60–70 dB) and the seismic to acoustic conversion at Anatahan should be efficient and aided by the upward slope of the seamount toward the hydrophone.

Fig. 4. Spectrograms (0–110 Hz) of hydrophone data in increments of an hour during the onset of the Anatahan eruption on 10 May 2004. Seismicity from Anatahan can be seen as the impulsive, short-duration signals at with peak acoustic energy in the range of 3–50 Hz. Hydrophone detected seismicity associated with the eruption begins between 0100Z and 0200Z and increases in intensity at ~06:20Z. The Volcanic Ash Advisory Center estimates, from satellite imagery, the eruption initiated around 0730Z, while broadband seismometers and long-period tiltmeters on Anatahan indicate the eruption seismicity and deformation began at ~0620Z and 0600Z, respectively (Wiens et al., 2004).

signal frequency of 10 Hz (optimum S to N frequency range for *T*-waves; Dziak et al., 1997) and the velocity model shown in Fig. 3b with sound channel axis of 800 m (Davis et al., 1986). The PE model indicates acoustic attenuation expected along the propagation path is relatively low (60–70 dB) and seems to generally be aided by the slope of Anatahan's flanks. The shape of the bathymetry along the flanks of Anatahan, from the sea surface to where the seafloor once again becomes horizontal some distance from the volcano, forms a concave up profile that will tend to focus acoustic energy upward into the water column and toward the sound channel thus enhancing signal detection by the hydrophone.

In addition to the seismo-acoustic phases that exit the volcano edifice and propagate directly into the sound channel, earthquakes from within Anatahan also generate seismic phases that propagate along the Moho discontinuity (*Pn*) and convert to an acoustic phase directly beneath the hydrophone (Dziak et al., 2004). These phases propagate at *P*-wave seismic speeds for the majority of the path to the hydrophone and thus arrive 7–8 min before the *T*-wave arrival at the hydrophone 300 km away (Figs. 2b and 4). Although *Pn* arrivals are not a large component of the hydrophone records from Anatahan, they are readily identifiable in the hydrophone records as the much lower frequency (<5 Hz) arrivals than the *T*-waves (3–50 Hz).

4. Hydrophone records of eruption seismicity

Fig. 4 shows spectrograms (frequency–time) of the hydrophone data during the onset of the Anatahan eruption from 0100Z to 1800Z on 10 May 2003. The apparent optimal seismic to acoustic conversion properties of Anatahan volcano should mean the hydrophone detected much of the small magnitude seismicity associated with the 10 May eruption. This seems to be the case because seismicity detected by a broadband IRIS/PASSCAL seismograph installed on Anatahan just 4 days prior to the eruption (Wiens et al., 2004) was also detected by the hydrophone despite the hydrophone being ~300 km from the volcano. The hydrophone does record infrequent seismicity in the days preceding the eruption, although there were no obvious indications an
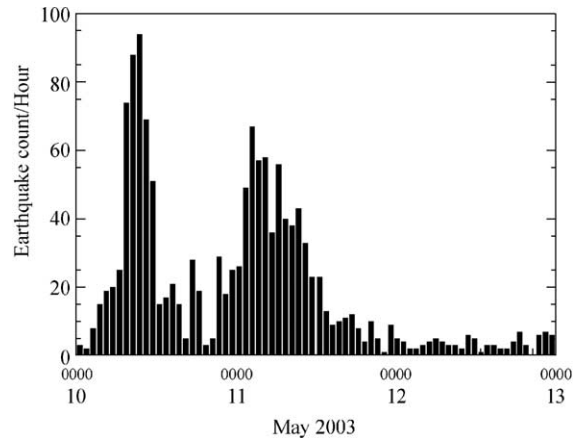

Fig. 5. Diagram shows the number of earthquakes per hour during the eruption. The hydroacoustic earthquake activity was a maximum between 0600 and 0800Z on 10 May as well as 16 h later at 0100–0300Z on 11 May.

eruption was imminent. Since it is, however, not possible to locate earthquakes nor derive a back-azimuth to the earthquake signal source with this one hydrophone, the origin of the hydrophone-recorded seismicity preceding the eruption remains ambiguous. There are also ocean bottom hydrophones deployed near Palau and Taiwan (operated by the Earthquake Research Institute of Japan and the Institute of Earth Sciences in Taiwan) that are between 1600 and 2300 km to the southwest and northwest of Anatahan. Review of the records indicates the eruption signals were not recorded on these hydrophones, indicating the acoustic signals from the eruption were not exceptionally energetic. Additionally, it seems likely the South Honshu Ridge, the seamount chain that forms a bathymetric shallows to the west of the Mariana Islands and our hydrophone deployment location, may have blocked acoustic energy from the Anatahan eruption from being recorded by the Palau and Taiwan hydrophones.

A total of 1401 earthquakes were recorded on our near CNMI hydrophone during the first 3 days of the eruption (Figs. 4 and 5). The hydrophone records show the same general increase in seismicity leading up to the eruption as recorded by the broadband seismometers. The first few earthquakes occur between 0100 and 0200Z on 10 May and an increase of seismicity begins about 4–5 h later at 0620Z (Wiens et al., 2004). The hydrophone

apparently recorded significantly more earthquakes than the seismometer on Anatahan Island which again could be a result of the efficient seismic to acoustic conversion from the volcanic edifice into the ocean sound channel. A long-period tiltmeter also on the island detected the first deformation signal from the eruption at 0600Z, while the Volcanic Ash Advisory Center estimates the eruption initiated at 0730Z from satellite images of the ash cloud (Wiens et al., 2004). A histogram of the number of earthquakes through time indicates seismicity was a maximum (>60 events/h) between 0600–0800Z on 10 May as well as 16 h later during 0000–0200Z on 11 May 2004. The earthquake activity decreased rapidly afterward to a few events per hour by the end of 11 May.

5. Earthquake depths

Focal depths derived from the seismic records of 13 earthquakes recorded during the Anatahan eruption from 10–13 May ranged from 8.1 to 13.3 km (D.A. Wiens, personal communication). Although there is not yet a method to directly estimate the depth of an earthquake from the acoustic (*T*-wave) signal, the rise time (Fig. 6), or the time from the emergence of the *T*-wave signal above ambient noise to the peak amplitude of a hydroacoustic envelope, has been shown to be a proxy for the relative depths of earthquakes (Schreiner et al., 1995; Yang and Forsyth, 2003). A decrease in rise times has been interpreted to reflect shoaling of a dike as it propagated along a rift zone (Schreiner et al., 1995; Dziak and Fox, 1999), with spatio-temporal clustering of earthquakes with very short rise times (<10 s) representing actual magma eruption onto the seafloor. Yang and Forsyth (2003) developed synthetic models of *T*-wave packet rise times and showed for focal depths of 1, 3 and 6 km that rise times will increase by several seconds with increasing earthquake depth. The Anatahan earthquakes with focal depths of 8.1–13.3 km had rise times ranging from 13.7 to 29.8 s. Thus the rise times from the eruption indicate (Fig. 7) that many earthquakes were relatively shallow (10–40-s rise times) at the onset of the volcanic activity at 0200Z and throughout the eruption on 10–13 May. Overall, however, the increase in seismicity associated with the
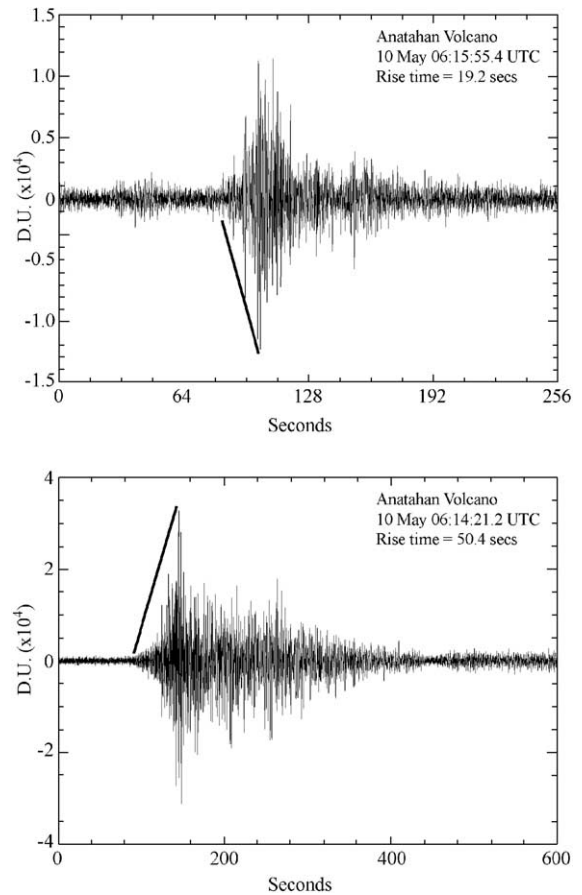

Fig. 6. Example time-series showing the T-wave signal packets of two earthquakes that occurred within Anatahan Volcano. The top earthquake is an example of a relatively short rise-time (shallow hypocenter), bottom event has a relatively long rise-time (deep hypocenter). Both earthquakes occurred during the first day of the eruption. Heavy black line shows the "rise" of the *T*-wave signal packet from the onset on the left to the maximum amplitude on the right. D.U. is digital units.

eruption at 0600–0800Z also corresponds to the time of largest rise times (>40 s) and therefore the largest relative earthquake depths. Similarly, the peak in earthquake activity observed 16 h after the main eruption activity at 0000–0200Z on 11 May corresponds to an increase in the depths of earthquakes as well. This indicates that the 11 May activity was a major explosion/eruption event similar, but likely not as large, as the initial eruption at 0600Z on 10 May. In addition there is evidence of very deep earthquakes (>100-s rise times) that occurred during the first 12 h of the eruption as well as during the second increase
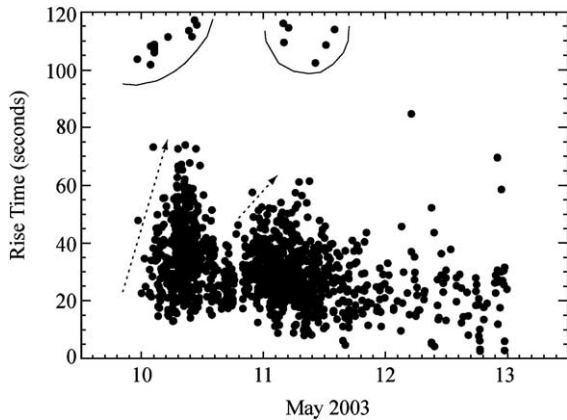
Fig. 7. Variation of earthquake rise times during the first 3 days of the Anatahan eruption. A significant number of earthquakes have short (10–40 s) rise times (shallow depths). Overall, however, the hydrophone-recorded earthquakes show a steady increase in rise times (dashed arrows) indicating an increase in relative earthquake depths during the onset of the eruption during 0200–0800Z on 10 May and once again from 1600 on 10 May to 0100Z on 11 May. There are also several very deep (>100-s rise times highlighted with grey lines) associated with the first 12 h of the eruption, as well as during the second increase in activity on 11 May, perhaps associated with magma emplacement from deep beneath Anatahan.

in seismic activity on 11 May. These deep events may reflect the emplacement of magma into the shallow volcanic edifice from deep beneath Anatahan during the initial phase of the eruption. It is not known what depth of earthquake produces T-wave rise times of >100 s, but these times seem to imply the earthquakes are at least twice as deep (>20–25 km) as the 40-s rise time events. The rise times also become progressively more shallow (<10 s) over the 3 days of activity, perhaps reflecting explosion/faulting activity near the surface of the caldera floor in response to shallow magma emplacement during the eruption.

6. Volcanic tremor

A broadband, continuous tremor-like energy accompanies the onset of increased seismicity at 0620Z on 10 May during the Anatahan eruption. Intrusion tremor observed at Krafla Volcano in Iceland is very similar to the tremor observed here, with a broad spectrum and dominant frequencies >3 Hz (Brandsdottir and Einarsson, 1992). Intrusions of magma dikes at Krafla generally are accompanied

by this broadband tremor mixed with swarms of small earthquakes both of which usually stop when the magma reaches the surface or the dike stops propagating. Fig. 8 shows the detailed spectra of an earthquake, volcanic tremor, and ambient noise from the hydrophone during the peak of eruption activity at 0700Z on 10 May. If the tremor signal is a result of magma injecting through the crust and not simply reverberation (reflection/refraction) of earthquake acoustic signals in the water column, then it should have a different frequency content than the earthquakes. There is clear broadband energy present on the hydrophone from 3 Hz up to at least 40 Hz that is distinct from the spectral content of the earthquakes and significantly above ambient noise. The tremor and earthquake also have different dominant frequencies as well as distinctly different overall levels of relative amplitude, although their overall bandwidths appear to be the same. Since volcanic tremor normally has much lower source energy than earthquakes (Chouet, 1992), the difference in spectral amplitudes does not
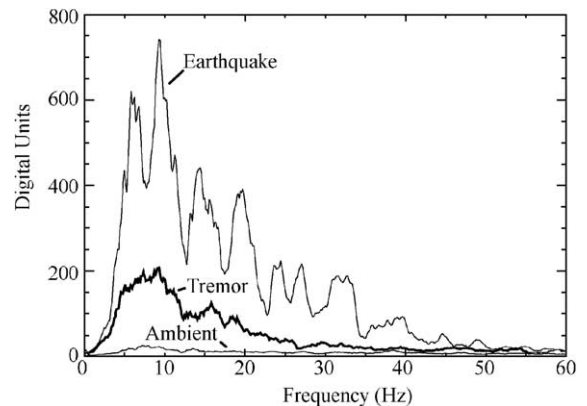

Fig. 8. Diagram shows detailed spectra of an earthquake, volcanic tremor, and ambient noise from the hydrophone during the peak of earthquake activity at 0700Z on 10 May. If the tremor signal is a result of magma injecting through the crust and not simply reverberation (reflection/refraction) of the earthquake signal in the water column, then it should have a different frequency content than the earthquakes. The tremor and earthquake have different dominant frequencies, although their overall bandwidth appears to be similar. There are, however, distinct peaks in the earthquake frequency spectrum beginning at 5 Hz and progressing at ~5-Hz intervals that are not readily apparent in the tremor spectrum. These peaks are very likely resonances of the 5-Hz earthquake acoustic signals, where the wavelength of a 5-Hz signal in water is 300 m and the ocean is 4500 m (15 wavelengths) deep.

help address the question of the tremor's source. Additionally if the energy is from reverberation, the amplitudes should also be lower due to signal attenuation. The timing of the broadband energy is, however, an important observation in that it occurs during the period of main eruption activity (0600–1000Z on 10 May) and is not seen at any other time. Thus the evidence provided here indicates the broad-band tremor-like energy is significant and although it may in part be due to reverberation of the earthquake acoustic signals through the water column, the occurrence of this energy during the main intrusion/eruption episode on 10 May and its similarity to tremor observed at other volcanic systems is consistent with a magmatic origin. In addition, there are distinct peaks in the earthquake frequency spectrum in Fig. 8 beginning at 5 Hz and progressing at ~5-Hz intervals that are not readily apparent in the tremor spectrum. Since the water depth between Anatahan and the hydrophone stays at or near 4500 m for the entire distance, these peaks are very likely resonances of the 5-Hz earthquake acoustic signals, where the wavelength of a 5-Hz signal in water is 300 m and the ocean is 15 wavelengths deep. The lack of similar resonances in the tremor signal indicates that the tremor is not a result of reverberation of the earthquake energy in the water column.

7. Seismo-acoustic wavefield modeling

The physics of *T*-wave generation has been an active field of research since submarine earthquakes and volcanic eruptions were first detected throughout the Pacific Ocean basin using hydroacoustic methods in the 1950s. In regions of shallow sloping bathymetry, *T*-waves have been attributed to downslope propagation (e.g. Talandier and Okal, 1998). As an alternative, excitation through scattering from a rough seafloor has also been proposed as a mechanism for generating *T*-waves (De Groot-Hedlin and Orcutt, 1999, 2001; Park et al., 2001). This mechanism can be used to model not only slope-derived *T*-waves, but also the abyssal signals that are not explained readily by downslope propagation. Recent models have shown earthquake source-mechanism dependence of *T*-wave generation (Park et al., 2001) which seems to be supported by observational data (Dziak, 2001).

Earthquake and volcanic tremor *T*-waves associated with magma-dike injection events in the North-east Pacific ocean have been well documented (Dziak et al., 1995, 1996). Volcano-tectonic (VT) seismicity is often the first sign of renewed volcanic activity, and some eruptions have been immediately preceded by strong short-term increases in volcano-tectonic activity (Chouet, 1996). In contrast to VT activity, which is generally more spread out in space and time, long-period (LP) events and tremor activity originate in particular locations within the magma plexus where disturbances in the flow are encountered. LP/tremor events associated with submarine volcanic systems tend to occur at magnitudes below 4 (Einarsson, 1991) and they are rarely detected by land-based seismic networks. Many LP/tremor events have been recorded as *T*-waves on hydrophones in the north and western Pacific (Dziak et al., 1996; Dziak and Fox, 2002). However, the physics of volcanogenic T-wave generation is still not well understood because the basic element of LP/tremor activity is not brittle rock failure, but the underlying pressurization of magmatic and/or hydrothermal fluids and attendant pressure perturbations (Chouet, 1986). Currently, there is no theoretical/analytical solution to explain oceanic *T*-wave generation from a fluid-driven volcanic source.

At the end of this section, we present preliminary numerical results that show the efficiency of oceanic *T*-wave generation from a volcanic source through seismic-wave scattering due to seafloor roughness. Although there are many possible geometries for volcano resonators such as fluid-filled pipes (Chouet, 1985), spheres (Crosson and Bame, 1985) and cracks (Aki et al., 1977; Chouet, 1986, 1988), we chose to use the fluid-filled pipe model because it allows for a more straightforward relation between volcano geometry and spectral features of harmonic tremor as well as its morphologic similarity to a submerged volcanic edifice.

A modal representation of the seismo-acoustic wavefield provides a natural framework for modeling *T*-waves. Modal analysis clearly presents well known features of the *T*-wave signal packet including the generally weak dispersion and the concentration of energy near the sound channel axis as well as providing insights into *T*-wave source mechanisms (Park and Odom, 1999). We will now derive the

analytical solution for a fluid-filled pipe source model which can be used to model the generation of volcanogenic *T*-waves and eventually (although outside the scope of this study) to compute synthetic *T*-wave signals and spectrograms. These representations are based on previously developed mode scattering models (Park and Odom, 1999) and seismo-acoustic excitation mechanisms (Park et al., 2001).

7.1. Fluid-filled pipe model

Chouet (1985) developed a fluid-filled pipe model to explain the mechanisms of a volcanic eruption. We follow directly the derivation of Chouet (1985) where the pipe model consists of three source parts; trigger, cylinder and disk (Fig. 9). The displacement of the
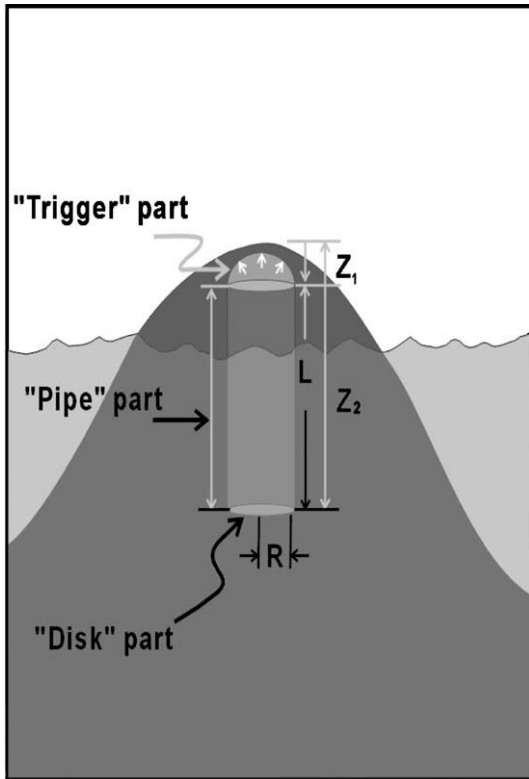

Fig. 9. Diagram illustrating the buried magma pipe model within a partially submerged volcanic edifice. The locations of the trigger, pipe and disk sections of the model are shown. R is the radius of the pipe, L is vertical pipe length, Z_1 is the depth to the pipe inlet and Z_2 is the total depth of the pipe.

seismo-acoustic wavefield for the trigger part can be represented as:

$$u_z(r,z;\omega) = \sum_q \frac{r_2(z,k_q)}{2cUI_1} \sqrt{\frac{2\pi}{k_q r}} S(\omega) e^{i(k_q r - \frac{\pi}{4})}$$
$$\times [2\mu k_q r_1(z_s,k_q) + r_4(z_s,k_q)], \qquad (1)$$

$$u_r(r,z;\omega) = \sum_q \frac{ir_1(z,k_q)}{2cUI_1} \sqrt{\frac{2\pi}{k_q r}} S(\omega) e^{i(k_q r - \frac{\pi}{4})}$$
$$\times [2\mu k_q r_1(z_s,k_q) + r_4(z_s,k_q)], \qquad (2)$$

where U and I_1 are the group velocity and an energy integral of Rayleigh waves, respectively, and r is the distance from the pipe to the hydrophone receiver and r_1, r_2, r_3, and r_4 are used to represent the initial excitation of eigenfunctions for Rayleigh waves (Aki and Richards, 1980). The source term is given by:

$$S(\omega) = \frac{P(R,\omega)R^3 e^{i(k_\alpha R - \delta)}}{4\mu \left[\left(1 - \frac{k_\beta^2 R^2}{4}\right)^2 + k_\alpha^2 R^2 \right]^{\frac{1}{2}}}, \qquad (3)$$

$$\delta = \tan^{-1} \frac{k_\alpha R}{1 - \left(\frac{k_\beta^2 R^2}{4}\right)}. \qquad (4)$$

With $P(R,\omega)$ representing the Fourier transform of the pressure applied at the cavity wall which is a function of both R, the radius of the pipe, and ω which is signal frequency. δ represents a phase shift in the conversion from compressional to shear waves. The wave numbers in Eqs. (3) and (4) are given by:

$$k_\alpha = \frac{\omega}{\alpha}, \quad k_\beta = \frac{\omega}{\beta}, \qquad (5)$$

where α and β are the compressional and shear wave velocities in the volcanic crust. The displacement in the cylinder part of the pipe model is:

$$\mathbf{u}(x,z;\omega) = \sum_q c_q(x)\mathbf{u}^q(z,k_q;x) e^{i \int_{x_s}^{x} k_q(\varsigma) d\varsigma}, \qquad (6)$$

and the initial excitation is:

$$c_q(x = x_s) = \pi R S_2(\omega) \times \left[k_q(\lambda + 2\mu)r_1(z_s,k_q) \right.$$

$$+ k_q \frac{\lambda^2}{\lambda + 2\mu} r_1(z_s,k_q)$$

$$\left. + \frac{\lambda}{\lambda + 2\mu} r_4(z_s,k_q) \right], \qquad (7)$$

where λ and μ are Lame constant and rigidity modulus and the source term is given by:

$$S_2(\omega) = \frac{P_0 R}{2\mu\xi} \times \left[\sinh(\xi z_1 + \xi L) - \sinh(\xi z_1) \right.$$
$$- \frac{Z_H \sinh(\xi L) + Z_C \cosh(\xi L)}{Z_H \cosh(\xi L) + Z_C \sinh(\xi L)}$$
$$\left. \left\{ \cosh(\xi z_1 + \xi L) - \cosh(\xi z_1) \right\} \right], \qquad (8)$$

where ξ is the complex wave number of the acoustic pressure waves in the fluid-filled pipe. The terms Z_H and Z_C are the hydraulic impedance and the characteristic impedance, respectively:

$$Z_H = \frac{P_L}{V_L}, \quad Z_C = \frac{\rho a^2 \xi}{s} \qquad (9)$$

where P_L and V_L are pressure and velocity at the bottom of the cylinder, and s is complex frequency, and a is acoustic velocity within the tube, i.e., acoustic pressure wave-speed in a magma melt. The sound velocity within a melt is given by Ferrick et al. (1982):

$$a = \left(\frac{K/\rho}{1 + (2K/\mu_c)(1 + v_c)} \right)^{1/2}, \qquad (10)$$

where ρ and K re the fluid density and bulk modulus of a magma melt, respectively, and μ_c and v_c are the modulus of rigidity and Poisson's ratio of the conduit. Murase and McBirney (1973) experimentally determined the fluid density ρ, viscosity η, bulk modulus K, and pressure wave speed of an andesitic melt. The melt was entirely fluid at temperatures greater than 1200 °C. For an assumed temperature of 1250 °C, the parameter values were given as $\rho = 2430$ kg/m^3, $\eta = 1 \times 10^3$ Ns/m^2, $K = 1.78 \times 10^{10}$ Pa, and the acoustic wave speed $a = 2700$ m/s. Ferrick et al. (1982) used these melt values to model the fluid-dynamic source mechanism of low-frequency volcanic tremor. Chouet (1985), however, chose parameter values representative of a dacitic magma, consistent with the composition of Anatahan volcano, for modeling volcanic tremor using values of $\rho = 2700$ kg/m^3, $\eta = 2 \times 10^5$ Ns/m^2, $K = 1.78 \times 10^{10}$ Pa and $a = 1600$ m/s. The Chouet (1985) estimate of the fluid viscosity is 2 orders of magnitude larger than Ferrick et al. (1982). In view of such a large variation in

magma viscosities, the estimate of Chouet (1985) consistent with a dacitic composition is considered as the more appropriate value for Anatahan magma.

Based on the above analytical solution, we then developed a numerical code to show T-wave generation via seafloor scattering of the seismo-acoustic wavefield using the trigger part of the pipe model as the source. Our preliminary results are presented in the following section.

7.2. Seismo-acoustic normal modes and T-wave excitation

The initial seismo-acoustic wavefield was generated using the trigger part of the fluid-filled pipe model for Anatahan Volcano (Fig. 9). The volcano source was assumed to be 1100 m below sea level. The same volcanic source parameters as Chouet (1985) were used since they are representative of a dacitic magma. The trigger part of the pipe model requires a relatively small number of source parameters, the pressure difference $\Delta P = 10^6$ dyn/cm and the radius of pipe $R = 25$ m, as compared to a more sophisticated pipe segment of the source model. We assume that the tangent of sloping seafloor is one (i.e., 45° slope) and the RMS height of fine-scale roughness of seafloor is 1 m (Park et al., 2001).

Seismo-acoustic normal modes were computed at two points, the submarine flank of Anatahan Volcano and the hydrophone location, using DISPER80 (Saito, 1988). Our earth model consists of an overlying ocean, seafloor sediments, ocean crust and upper mantle. The model at the volcano flank includes a 1000-m-deep water column, while the model at the hydrophone includes a 4437-m water column. For the volcano flank, 104 seismo-acoustic modes were computed at 10 Hz. The first 12 overtones are acoustic modes whereas the higher-order modes are mostly crustal modes (Fig. 10a–d). For the earth model at the hydrophone, a total of 133 seismo-acoustic modes were computed at 10 Hz. The first 50 overtones are acoustic normal modes, which propagate in the water column as acoustic guided waves trapped in the ocean sound channel. Fig. 11a–d shows the amplitudes of the 1st, 15th, 32nd and 50th overtones, which are examples of ocean acoustic modes. The 50th overtone (Fig. 11d) starts to show
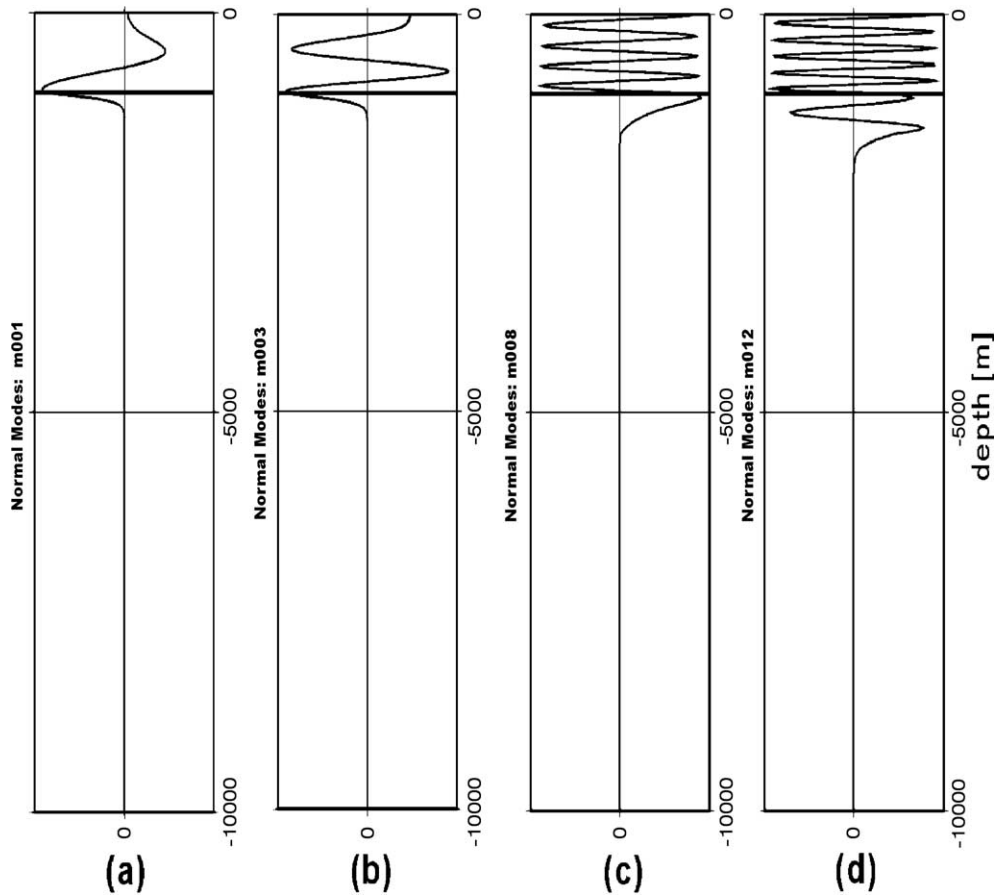
Fig. 10. Seismo-acoustic normal modes computed for the ocean–crust model of the submarine flank of Anatahan Volcano at 10 Hz. (a) the 1st overtone (b) 3rd overtone (c) 8th overtone and (d) 12th overtone. Solid horizontal line represents the seafloor at a depth of ~1000 m below sea level.

characteristics of ocean crustal modes as well as acoustic modes.

Seafloor earthquakes initially generate crustal seismic waves that transfer their energy from the higher order crustal modes to the Stoneley fundamental waves at the seafoor–ocean interface. These Stoneley interface waves then convert to the lower order acoustic modes (T-waves) that propagate within the ocean water column through scattering along a rough seafloor (Park et al., 2001). The T-wave source mechanisms, as well as the ocean crust geometry of the partially submerged Anatahan Volcano, are different from those of T-waves generated by typical ocean crust earthquakes. A shallow triggering source inside the volcanic edifice effectively excites acoustic waves at the submarine flank of the volcano (Fig. 12a), there-fore a significant portion of the initial seismo-acoustic wavefield energy is acoustic normal modes, which can directly propagate into the ocean-sound channel. In addition to this initial acoustic wave excitation, seafloor scattering further enhances energy conversion from crustal modes to the lower acoustic modes propagating in the water column (Fig. 12b). Thus Anatahan, as well as other similarly shaped submarine volcanoes, provides highly efficient conversion of seismic to acoustic energy enhancing remote detection of T-waves from earthquakes associated with seafloor volcanic activity. The goal of the numerical modeling effort presented here was to demonstrate the efficiency of T-wave generation from seismic wave scattering as well as to provide some insights into possible source geometries as well as into properties of the magma.
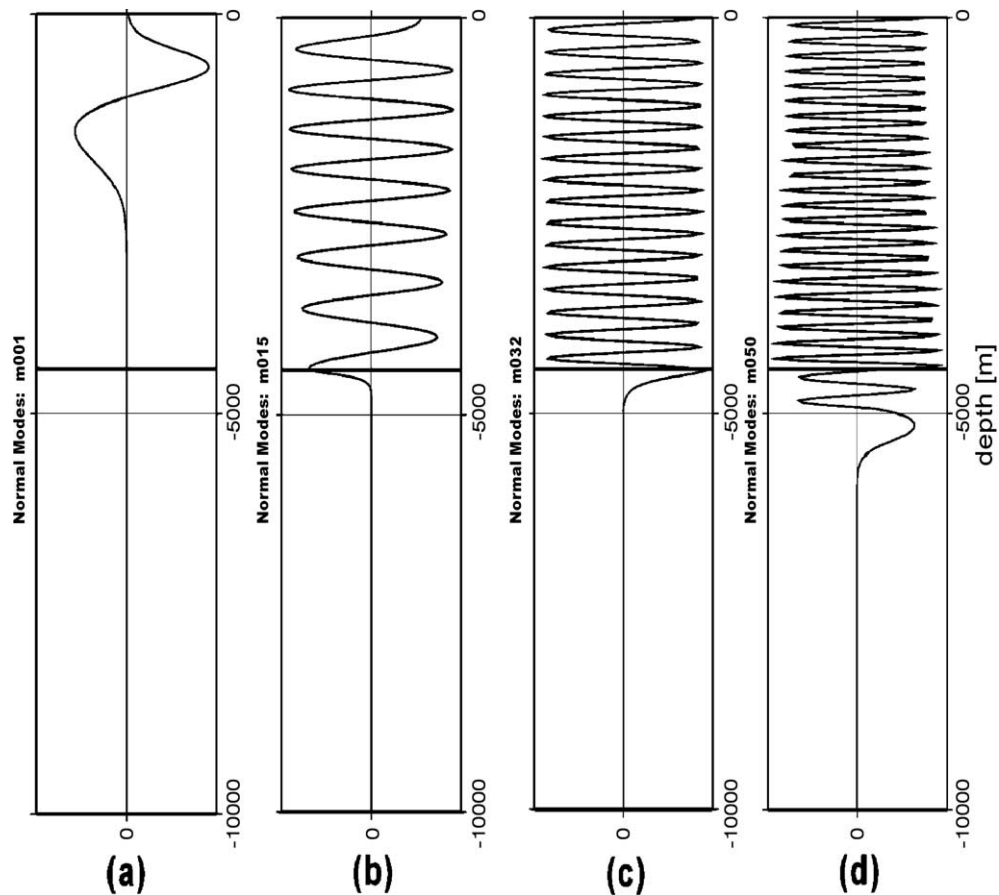
Fig. 11. Seismo-acoustic normal modes computed for the ocean–crust model near the hydrophone location at 10 Hz. (a) the 1st overtone (b) 15th overtone (c) 32nd overtone and (d) 50th overtone. Solid horizontal line represents seafloor at a depth of ~4437 m below sea level.

Comparison of model *T*-wave signals to actual data is beyond the scope of this presentation, but will be the focus of studies in the near future.

8. Summary

An autonomous hydrophone moored in the sound channel ~300 km from Anatahan Volcano clearly recorded seismicity and volcanic tremor associated with the 10 May 2003 explosive eruption. Seismic activity from Anatahan observed on the hydrophone was first recorded between 0100 and 0200Z on 10 May, with earthquake activity significantly increasing at ~0620Z on 10 May, similar to the timing of seismic activity observed by a broadband seismograph station on the island and the creation of an ash cloud detected

by satellite monitoring systems. A total of 1401 earthquakes were detected on the hydrophone during the onset and first 3 days of the eruption. Seismicity was at a maximum (50 events/h) at 0800Z on 10 May as well as 16 h later during 0000–0200Z on 11 May 2003, indicating there were two main periods of explosion/eruption activity. Relative earthquake depth estimates indicate that both eruption periods were accompanied by earthquake activity from deep within the Anatahan volcanic edifice. The earthquake activity decreased rapidly after the second peak in seismic activity to a few events per hour by the end of 11 May. The period of peak earthquake activity between 0600 and 1000Z on 10 May was accompanied by continuous, low-frequency (3–40 Hz) energy that is consistent with volcanic (intrusion) tremor observed at other volcanic systems. A numerical representation of
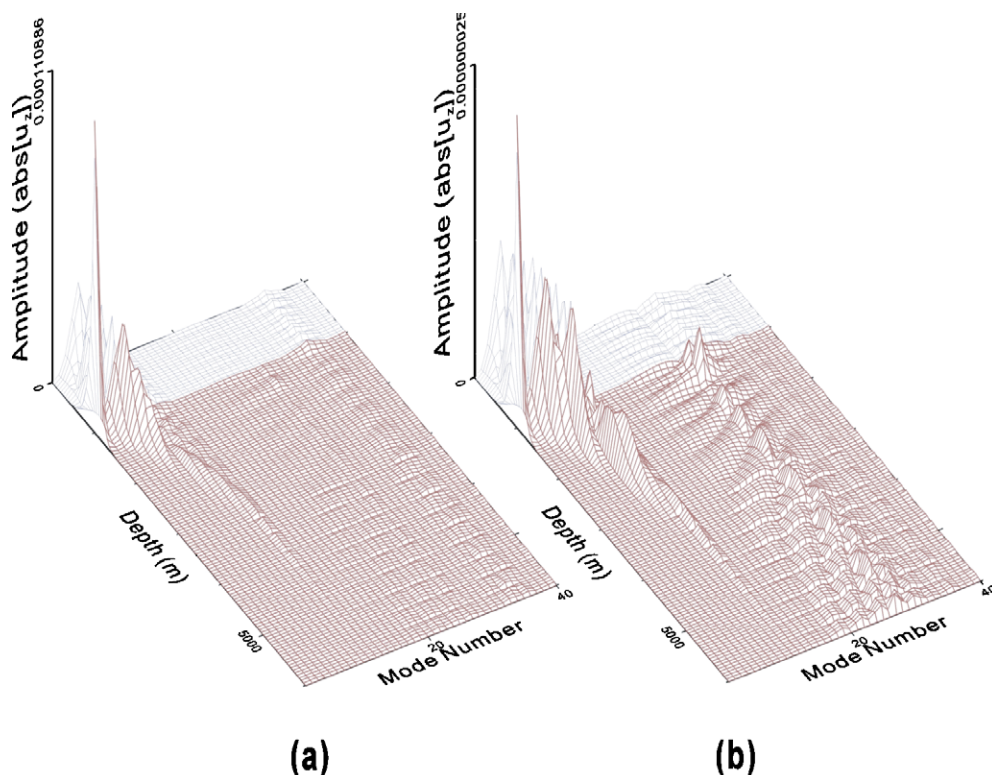
Fig. 12. Seismo-acoustic wavefield computed at the submarine flank of Anatahan Volcano using the buried magmatic pipe model. (a) Initial seismo-acoustic wavefield and (b) scattered wavefield.

the Anatahan volcano-seismic source was developed to examine the character of acoustic signals generated from the eruption governed by the geometry of the source and the physical properties of the magma. A magma pipe source mechanism was used to compute the seismo-acoustic wavefield on the flank of the Anatahan volcanic edifice (on the seafloor and in the water column) due to mode conversion by roughness scattering. A fluid-filled pipe model was chosen because it allows for a more straightforward relation between volcano geometry and spectral features of harmonic tremor as well as its morphologic similarity to a submerged volcanic edifice. A flank source was found to be very efficient at transferring energy from the initial seismo-acoustic wavefield into the acoustic normal modes that propagate within the ocean-sound channel. Thus hydroacoustic monitoring techniques offer a highly effective method for detecting magmatic activity from submarine/subaerial island-arc volcanoes.

Acknowledgements

References

Aki, K., Richards, P.G., 1980. Quantitative Seismology, 2 volumes. W.H. Freeman and Company, New York, NY (932 pp.).
Aki, K., Fehler, M., Das, S., 1977. Source mechanism of volcanic tremor: fluid-driven crack models and their applica-

tion to the 1963 Kilauea eruption. J. Volcanol. Geotherm. Res. 2, 259–287.

Brandsdottir, B., Einarsson, P., 1992. Volcanic tremor and low-frequency earthquakes in Iceland. In: Gasparini, P., Scarpa, R., Aki, K. (Eds.), IAVCEI Proceedings in Volcanology. Springer-Verlag, Berlin, Germany, pp. 212–222.

Bulletin of the Global Volcanism Network, v:28, 5, May 2003.

Chouet, B., 1985. Excitation of a buried magmatic pipe: a seismic source model for volcanic tremor. J. Geophys. Res. 90, 1881–1893.

Chouet, B., 1986. Dynamics of a fluid-driven crack in three dimensions by the finite difference method. J. Geophys. Res. 91, 13967–13992.

Chouet, B., 1988. Resonance of a fluid-driven crack: radiation properties and implications for the source of long-period events and harmonic tremor. J. Geophys. Res. 93, 4375–4400.

Chouet, B., 1996. Long-period volcano seismicity: its source and use in eruption forecasting. Nature 380, 309–316.

Chouet, B.A., 1992. A seismic model for the source of long-period events and harmonic tremor. In: Gasparini, P., Scarpa, R., Aki, K. (Eds.), Volcanic Seismology. Springer-Verlag, Berlin, pp. 133–156.

Collins, M.D., 1993. A split-step Padei solution for the parabolic equation method. J. Acoust. Soc. Am. 93, 1736–1742.

Crosson, R.S., Bame, D.A., 1985. A spherical source model for low frequency volcanic earthquakes. J. Geophys. Res. 90, 10237–10247.

Davis, T.M., Countryman, K.A., Carron, M.J., 1986. Tailored acoustic products utilizing the NAVOCEANO GDEM (a generalized digital environmental model). Proceedings, 36th Naval Symposium on Underwater Acoustics, Naval Ocean Systems Center, San Diego, CA.

De Groot-Hedlin, C., Orcutt, J.A., 1999. Synthesis of earthquake-generated T-waves. Geophys. Res. Lett. 26, 1227–1230.

De Groot-Hedlin, C., Orcutt, J.A., 2001. Excitation of T-phases by seafloor scattering. J. Acoust. Soc. Am. 109, 1944–1953.

Dziak, R.P., 2001. Empirical relationship of T-wave energy and fault parameters of Northeast Pacific Ocean earthquakes. Geophys. Res. Lett. 28, 2537–2540.

Dziak, R.P., Fox, C.G., 1999. Long-term seismicity and ground deformation at Axial Volcano, Juan de Fuca Ridge. Geophys. Res. Lett. 26, 3641–3644.

Dziak, R.P., Fox, C.G., 2002. Harmonic tremor from a submarine volcano detected across the Pacific Ocean basin. J. Geophys. Res. 29 (12). doi:10.1029/2001GL01391.

Dziak, R.P., Fox, C.G., Schreiner, A.E., 1995. The June–July 1993 seismo-acoustic event at CoAxial segment, Juan de Fuca Ridge; evidence for a lateral dike injection. Geophys. Res. Lett. 22, 135–138.

Dziak, R.P., Fox, C.G., Embley, R.W., Lupton, J.E., Johnson, G.C., Chadwick, W.W., Koski, R.A., 1996. Detection of and response to a probable volcanogenic T-wave event swarm on the western Blanco Transform Fault Zone. Geophys. Res. Lett. 23, 873–876.

Dziak, R.P., Fox, C.G., Matsumoto, H., Schreiner, A.E., 1997. The April 1992 Cape Mendocino earthquake sequence: Seismo-acoustic analysis utilizing fixed hydrophone arrays. Mar. Geophys. Res. 19, 137–162.

Dziak, R.P., Bohnenstiehl, D.R., Matsumoto, H., Fox, C.G., Smith, D.K., Tolstoy, M., Lau, T.-K., Haxel, J.H., Fowler, M.J., 2004. P- and T-wave detection thresholds, Pn velocity estimate, and detection of lower mantle and core P-waves on ocean sound-channel hydrophones at the Mid-Atlantic Ridge. Bull. Seismol. Soc. Am. 94 (2), 665–677.

Einarsson, P., 1991. Earthquakes and present-day tectonism in Iceland. Tectonophysics 189, 261–279.

Ferrick, M.G., Qamar, A., St.Lawrence, W.F., 1982. Source mechanism of volcanic tremor. J. Geophys. Res. 87, 8675–8683.

Fox, C.G., Dziak, R.P., Matsumoto, H., Schreiner, A.E., 1994. Potential for monitoring low-level seismicity on the Juan de Fuca Ridge using military hydrophone arrays. Mar. Technol. Soc. J. 27 (4), 22–30.

Fox, C.G., Matsumoto, H., Lau, T.K.A., 2001. Monitoring Pacific Ocean seismicity from an autonomous hydrophone array. J. Geophys. Res. 106, 4183–4206.

Kanamori, H., 1988. Ocean-floor seismic stations and source mechanism studies; broad-band downhole seismometers in the deep-ocean. Woods Hole Oceanogr. Inst. 82–83.

Murase, T., McBirney, A.R., 1973. Properties of some common igneous rocks and their melts at high temperatures. Geol. Soc. Amer. Bull. 84, 3563–3592.

Park, M., Odom, R., 1999. The effect of stochastic rough interfaces on coupled-mode elastic waves. Geophys. J. Int. 136, 123–143.

Park, M.-K., Odom, R., Soukup, D.J., 2001. Modal scattering: a key to understanding oceanic T-waves. Geophys. Res. Lett. 28 (17), 3401–3404.

Saito, M., 1988. DISPER80: a subroutine package for the calculation of seismic normal mode solutions. In: Doornbos, D. (Ed.), Seismological Algorithms: Computational Methods and Computer Programs. Academic Press, San Diego, pp. 293–319 (Chap. IV. 1).

Schreiner, A.E., Fox, C.G., Dziak, R.P., 1995. Spectra and magnitude of T-waves from the 1993 earthquake swarm on the Juan de Fuca Ridge. Geophys. Res. Lett. 22, 139–142.

Talandier, J., Okal, E.A., 1998. On the mechanism of conversion of seismic waves to and from T-waves in the vicinity of island shores. Bull. Seismol. Soc. Am. 88, 621.

Wiens, D.A., Shore, P.J., Sauter, A., Hilton, D.R., Fisher, T., Camacho, J.T., 2004. Observing the historic eruption of northern Mariana Islands volcano. Eos, Trans. Am. Geophys. Union 85 (1), 2–4 (6 January).

Yang, Y., Forsyth, D.W., 2003. Improving epicentral and magnitude estimation of earthquakes from T-phases by considering the excitation function. Bull. Seismol. Soc. Am. 93 (5), 2106–2122.